Migration regulates cellular mechanical states

Stephanie S. Chang†, Andrew D. Rape†, Stephanie A. Wong†, Wei-hui Guo, and Yu-li Wang*
Department of Biomedical Engineering, Carnegie Mellon University, Pittsburgh, PA 15213

ABSTRACT **Recent studies indicate that adherent cells are keenly sensitive to external physical environment, such as substrate rigidity and topography, and internal physical states, such as cell shape and spreading area. Many of these responses are believed to involve coupled output and input of mechanical forces, which may constitute the key sensing mechanism to generate downstream regulatory signals for cell growth and differentiation. Here, we show that the state of cell migration also plays a regulatory role. Compared with migrating cells, stationary cells generate stronger, less dynamic, and more peripherally localized traction forces. These changes are coupled to reduced focal adhesion turnover and enhanced paxillin phosphorylation. Further, using cells migrating along checkerboard micropatterns, we show that the appearance of new focal adhesions directly in front of existing focal adhesions is associated with the down-regulation of existing focal adhesions and associated traction forces. Together, our results imply a mechanism where cell migration regulates traction forces by promoting dynamic turnover of focal adhesions, which may then regulate processes such as wound healing and embryogenesis where cell differentiation must coordinate with migration state and proper localization.**

Monitoring Editor
Valerie Marie Weaver
University of California, San Francisco

Received: Feb 12, 2019
Revised: Oct 10, 2019
Accepted: Oct 28, 2019

INTRODUCTION

Accumulating evidence indicates that adherent cells are keenly sensitive to their own internal and external physical states. For example, elongated shape (Kilian *et al.*, 2010), large spread area (McBeath *et al.*, 2004), and rigid substrates (Engler *et al.*, 2006) all favor osteogenic differentiation, while opposite conditions favor adipogenic or neurogenic differentiation. In addition, conditions that favor osteogenic differentiation, such as higher substrate rigidity and larger spreading area, also promote the generation of stronger traction forces (Lo *et al.*, 2000; Wang *et al.*, 2002; Trichet *et al.*, 2012). Other physical parameters, such as aspect ratio (Rape *et al.*, 2011b) and substrate dimensions (Baker and Chen, 2012; Chang *et al.*, 2013), also profoundly affect traction forces and may affect cell function in a similar manner.

Although myosin II–dependent traction forces are commonly considered to be responsible for driving cell migration (Dembo and Wang, 1999; Morin *et al.*, 2014), they also serve an alternative purpose of sensing external or internal physical states (Lo *et al.*, 2000; Wang *et al.*, 2002; Discher *et al.*, 2005; Prager-Khoutorsky *et al.*, 2011; Rape *et al.*, 2011a; Baker and Chen, 2012; Trichet *et al.*, 2012; Chang *et al.*, 2013), possibly through cellular responses to counterforces and/or resulting strains (Vogel and Sheetz, 2006; Rape *et al.*, 2011a; Trichet *et al.*, 2012). Supporting the importance of mechanical sensing, lineage specification for stem cells is known to be dependent on myosin II activities (Engler *et al.*, 2006). Conversely, defective regulation of traction forces and/or mechanical sensing is speculated to contribute to the metastatic potential of cancer cells, as traction forces are often disorganized in transformed cells (Munevar *et al.*, 2001), showing an increase in magnitude with increasing metastatic potential (Kraning-Ruch *et al.*, 2012). In addition, cells expressing oncogenes were defective in their response to substrate rigidity (Wang *et al.*, 2000). These observations suggest that traction forces may serve as a universal switch for controlling cell differentiation and as a handle for identifying strategies for clinical intervention.

Given the role of traction forces in cell migration, it is reasonable to speculate that the state of cell migration may exert feedback regulation on traction forces and possibly downstream signaling events. In this study, we show that cell migration indeed has a profound effect on both traction forces and protein phosphorylation at focal adhesions. We further suggest that the mechanism may involve mechanical cross-talks between preexisting and newly

This article was published online ahead of print in MBoC in Press (http://www.molbiolcell.org/cgi/doi/10.1091/mbc.E19-02-0099) on November 6, 2019.

†These authors contributed equally to this work and are listed in alphabetical order.

*Address correspondence to: Yu-li Wang (yuliwang@andrew.cmu.edu).

Abbreviations used: EMCCD, electron-multiplying charge-coupled device; FAAS, focal adhesion analysis server; TIRF, total internal reflection fluorescence.

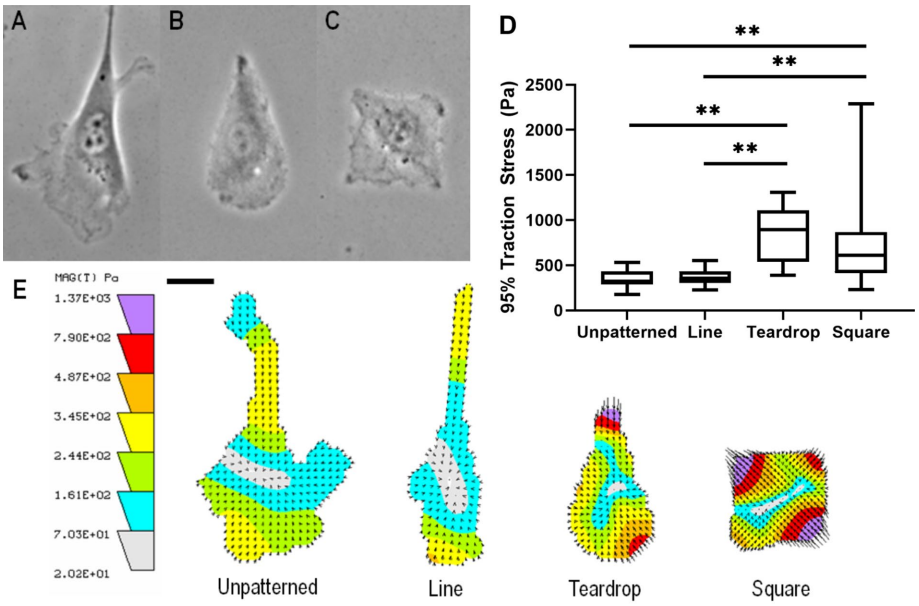

FIGURE 1: Traction force generation differs between migrating and stationary cells. NIH 3T3 cells were either allowed to migrate freely on a gel surface with a uniform coating of gelatin (A) or immobilized within gelatin-conjugated islands of teardrop (B) or square (C) shape. Graphs of the 95th-percentile traction stress exerted by migrating and stationary cells show that stationary cells exert approximately twice the traction stress of migrating cells regardless of the shape (D). $N = 18, 20, 15, 15$ for cells migrating on unpatterned surfaces, migrating along an adhesive strip, stationary within a square island, and stationary within a teardrop-shaped island, respectively. Representative heat maps of traction stress for migrating and stationary cells show that the strongest traction stress is located at the edge of stationary cells (E). Scale bars, 20 μm. Box-and-whisker plots show the median values, upper and lower quartile values, and maximal and minimal values (D). ** indicates $p < 0.05$.

formed focal adhesions to promote the turnover of focal adhesions and associated traction forces.

RESULTS

Stationary cells generate stronger traction stress than migrating cells

To investigate how traction stress distribution is affected by cell migration, we performed traction force microscopy on NIH 3T3 cells plated on elastic polyacrylamide gels with a Young's modulus of 3.5 kPa conjugated with gelatin on the surface to promote cell adhesion. Micropatterning of bound gelatin allowed precise control of cell size, shape, and migration state (Figure 1, A–C). Traction force generation was assessed based on the top five percentiles of traction stress, which concentrated near the front (Rape *et al.*, 2011b), to exclude background activities that covered most areas underneath a cell.

NIH 3T3 cells on a surface uniformly coated with gelatin migrated freely and exerted an average traction stress of 356 ± 25.6 Pa. Cells migrating along micropatterned strips of gelatin-conjugated substrate 30 μm in width exerted a similar traction stress of 370 ± 22.4 Pa. In contrast, when gelatin was micropatterned as 50 × 50–μm square islands to inhibit cell migration, stationary NIH 3T3 cells exerted a traction stress of 718 ± 124 Pa (Figure 1D). While previous studies have investigated cell migration in environments that limited cell spreading (Raman *et al.*, 2013), the current experimental setup allows direct comparison between migrating and stationary cells with similar spreading areas and aspect ratios (Figure 1, A–C). In this way, it is possible to unambiguously decouple the effects of migration on traction stress from other effectors that have been previously well characterized (e.g., cell size and cell shape). The twofold difference in traction stress between migrating and immobilized cells was unexpected because traction stress of stationary cells is known to increase with spreading size and aspect ratio (Rape *et al.*, 2011b), while cells on open surfaces may spread to a slightly larger size and higher aspect ratio than cells on 50 × 50–μm islands but showed a weaker traction stress (Supplemental Figure S1). Additionally, when plated on teardrop-shaped islands to mimic the shape and size of typical migrating cells, NIH 3T3 cells exerted a traction stress of 850 ± 81.9 Pa, similarly to those on square islands, which again argued against the effect of cell shape or spreading area and supported the notion that migration state regulates traction force generation.

Traction force heat maps further showed higher values along the edges of stationary cells than along those of migrating cells (Figure 1E). In addition, while spreading area and total strain energy were positively correlated for cells migrating on line substrates or unpatterned surfaces (Oakes *et al.*, 2014), cells on islands of either square or teardrop shape produced significantly higher strain energy than migrating cells of similar size (Supplemental Figure S2). Similar results were observed with RPE1 cells (Supplemental Figure S3), as well as NIH 3T3 cells plated on stiffer gels (Supplemental Figure S4), where they migrated at a speed of 19.4 ± 6.1 μm/h, lower than 23.6 ± 4.7 μm/h on soft gels.

Traction stress generation is dependent on cell migration speed

We next performed scatterplot analysis of 24 cells migrating at a speed of between 0 and 48 μm/h along adhesive strips 30 μm in width. As shown in Figure 2, traction stresses ranging between 300 and 900 Pa were negatively correlated with the speed of migration, even though these cells shared a similar shape. This analysis indicated that traction stress is negatively regulated by the speed of cell migration.

To further investigate the relationship between cell migration and traction force generation, we performed extended time-lapse

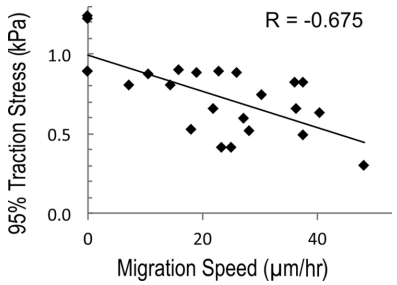

FIGURE 2: Traction force generation is regulated by cell migration state. Scatterplot analysis of 24 cells migrating along a 30 μm–wide adhesive strip shows that traction stress is negatively correlated with cell migration speed.

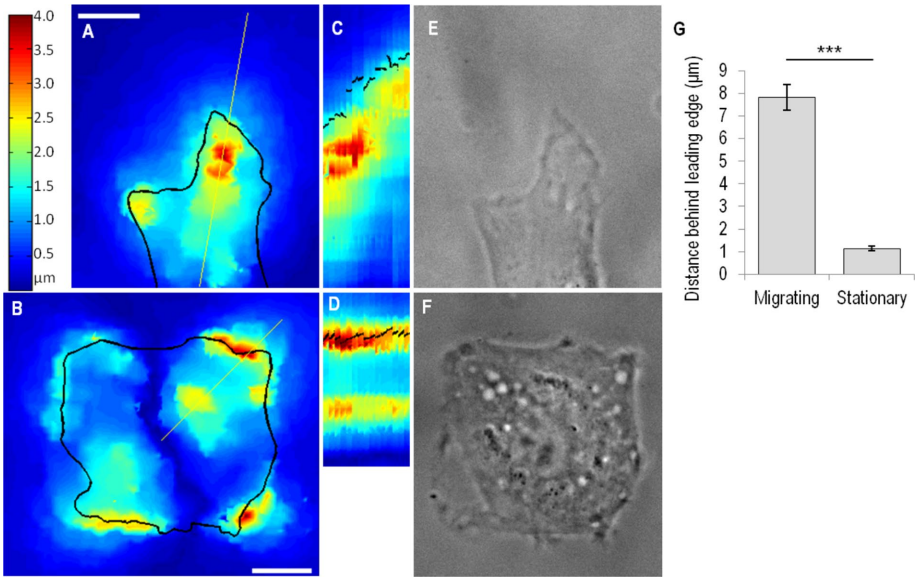

FIGURE 3: Substrate displacement heat maps at a high magnification (A, B) and the corresponding kymographs (C, D) and phase contrast images (E, F) reveal the location of maximal traction force relative to the leading edges of migrating (A, C, E) and stationary (B, D, F) cells. Scale bar, 10 μm. Black line represents cell outline. Thin yellow lines in heat maps (A, B) indicate the region of interest for generating kymographs (C, D). Note the steady association of maximal traction forces with the very edge of stationary cells but the constant distance from the leading edge in migrating cells (C, D, G). Substrate displacements are also larger and more persistent in stationary cells than in migrating cells. Kymograph duration, 1 h. Error bars represent SEM, and *** indicates $p < 0.001$.

traction force microscopy to track cells migrating on linear strips with a dead end, where cell migration typically paused for several hours before reversing direction (Supplemental Figure S5A). Traction stress increased approximately twofold as the cell paused at the end of the line (Supplemental Figure S5B), mirroring the twofold increase in traction stress of cells on micropatterned islands. A similar trend was observed for strain energy and total traction output (Supplemental Figure S5, C and E). As these cells showed a slight decrease in spreading area upon pausing (Supplemental Figure S5D), the results suggested that it is the state of cell migration rather than the cell area that caused the change in mechanical output.

Traction force distribution differs between stationary and migrating cells

The distribution of traction stress is known to differ from the distribution of total focal adhesions. Traction stress develops at newly formed focal adhesions near the leading edge, where its magnitude correlates positively with the size of focal adhesions, while large focal adhesions elsewhere often exert only weak traction stresses regardless of size (Beningo *et al.*, 2001; Stricker *et al.*, 2011). In stationary square-shaped cells, focal adhesions were found throughout the cell, while strong traction stress and ruffling activities were focused at corners (Parker *et al.*, 2002; Wang *et al.*, 2002).

We mapped the magnitude of substrate displacement at a high magnification to determine the location of the maximum relative to the leading edge in migrating and stationary cells (Figure 3, A and B). For stationary cells on square islands (Figure 3F), maximal substrate strain was found at the corners and along the very edges, as shown in the heat maps (Figure 3B). Notably, the site of high substrate strain was stationary and persisted for long periods of time (kymograph, Figure 3D). In contrast, for cells migrating either on an unpatterned surface or along 30-μm strips (Figure 3E), maximal substrate displacement was located on the average 8 μm behind the leading edge, which reflected the time required for the buildup of transient traction forces as the leading edge advanced (Figure 3G). In addition, maximal displacement showed a combination of dynamic forward movement and appearance of new sites as the leading edge migrated forward (Figure 3C).

Focal adhesion size and dynamics differ between stationary and migrating cells

Traction forces are generated by contraction of the actomyosin cytoskeleton and transmission to the substrate through integrins at focal adhesions (Beningo *et al.*, 2001; Geiger *et al.*, 2009; Vicente-Manzanares *et al.*, 2009). Staining of a myosin II regulatory light chain phosphorylated at Ser-19 showed a fourfold increase in intensity upon cell immobilization ($N = 16$ cells each), consistent with elevated myosin activity. We suspected that the difference in traction forces may be related to differences in the dynamics of focal adhesions. Using NIH 3T3 cells expressing mCherry–paxillin, we examined focal adhesions with total internal reflection fluorescence (TIRF) microscopy in cells plated on fibronectin-coated glass coverslips (Figure 4, A and B). Focal adhesions in square stationary cells showed only a slightly larger average size than those in migrating cells (0.52 vs. 0.47 μm^2; Figure 4E). However, focal adhesions at the corners of square cells, where the strongest traction forces were localized, were particularly prominent, showing an average area of 0.62 μm^2, with some exceeding 4 μm^2 (Figure 4, C and E). Time-lapse recording of migrating cells showed typical focal adhesion dynamics, forming at the leading edge, remaining largely stationary as the cell migrated forward, and disappearing as they became localized to the cell interior (Figure 4B). In contrast, most focal adhesions in cells on islands remained stationary relative to the substrate and showed a lifetime two times longer than those in migrating cells (Figure 4, B, D, and F). Curiously, a small fraction of focal adhesions were released from the edge and moved across a long distance toward the interior of the cell, as reported previously (long slanted streak in Figure 4D; Smilenov *et al.*, 1999).

Phosphorylation of Tyr-118 on paxillin is believed to represent part of the mechanotransduction mechanism at focal adhesions (Zaidel-Bar *et al.*, 2007; Choi *et al.*, 2011). To determine whether the differences in focal adhesion dynamics and mechanical activities between migrating and stationary cells were associated with changes in paxillin phosphorylation, NIH 3T3 cells on polyacrylamide gels were fixed and stained with polyclonal antibodies against paxillin phosphorylated at Tyr-118 (Figure 5, C and G) and counterstained with monoclonal antibodies against vinculin (Figure 5, A and E, magnified view in B and F). Fluorescence intensity of phosphorylated paxillin was normalized against vinculin intensity by ratio imaging (Figure 5, D and H). Phosphorylated paxillin was concentrated near the leading edges of migrating cells and along the edges of stationary cells. The intensity ratio was 68% higher in focal adhesions at the corners of stationary cells than in

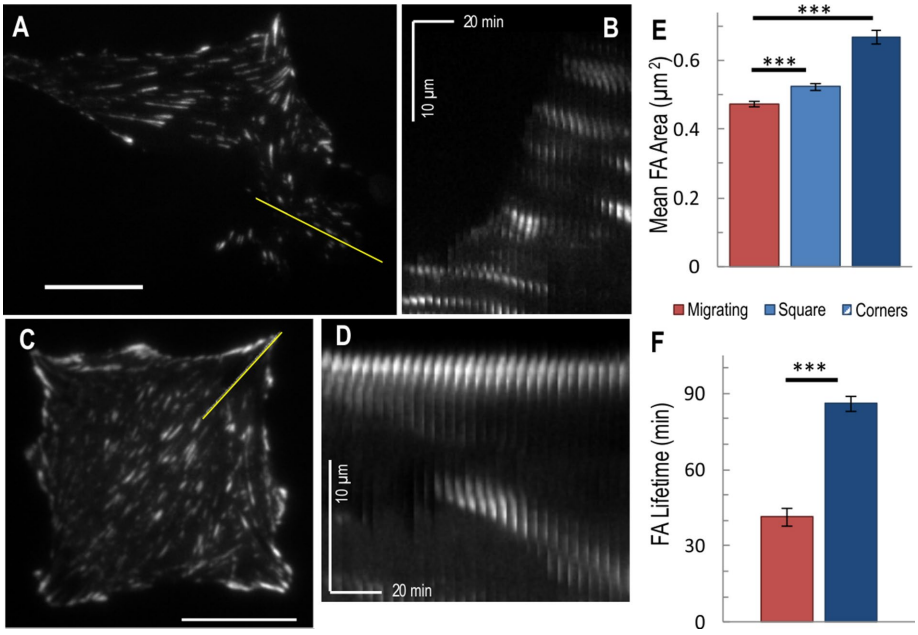

FIGURE 4: Focal adhesions are more dynamic in migrating (A) than in stationary (C) cells. NIH 3T3 cells expressing mCherry–paxillin and cultured on either unpatterned coverslips (A), or coverslips grafted with linear polyacrylamide to block cell adhesion outside square islands (C) are imaged with TIRF microscopy. Yellow lines indicate regions of interest for generating kymographs (B, D). Focal adhesions at the edge of stationary cells last much longer (C, kymograph in the right panel; D, bright horizontal band across the top) than focal adhesions in migrating cells (A, kymograph in the right panel; B, short streaks), consistent with the measurement of focal adhesion lifetimes (F; $N = 80$, 35 for focal adhesions in migrating and stationary cells, respectively). A small fraction of focal adhesions in stationary cells detached from the edge and moved across a long distance toward the cell interior (D, slanted streak; Smilenov *et al.*, 1999). Scale bar, 20 µm. Stationary cells show larger, more prominent focal adhesions than migrating cells, with particularly large adhesions found at the corners (E; $N =$ 4772, 4603, 1927 focal adhesions in migrating cells, square cells, and corners of square cells, respectively). Error bars represent SEM, and *** indicates $p < 0.001$.

those near the leading edge of migrating cells (Figure 5I), suggesting different signaling states between focal adhesions in stationary cells and migrating cells.

Mechanical output at existing focal adhesions are down-regulated as new adhesions form in front

We suspect that the difference in mechanical output between stationary and migrating cells may be due to the continuous protrusion and focal adhesion formation in front of preexisting focal adhesions in migrating cells. To address this possibility, cells were plated on a checkerboard micropattern where the leading edge might extend away from existing focal adhesions for up to 16 µm without the formation of new focal adhesions directly in front of existing adhesions (Figure 6A). Cells maintained a similar shape and speed when migrating on checkerboard pattern as on continuous lines (Supplemental Figure S6).

Time lapse recording of NIH 3T3 cells showed that substrate displacement persisted for a longer period of time when the leading edge migrated across a nonadhesive region (black arrow in kymograph, Figure 6B) than when it migrated along continuous lines (Figure 6C), despite similar cell morphology and migration speed (Supplemental Figure S6). The slower decay was also evident from the kinetics of substrate displacements (Figure 6, D and E), where cells on the checkerboard pattern sustained a longer duration of substrate strain (Figure 6F). Traction force microscopy further indicated that cells migrating on the checkerboard exerted 21% higher traction stress than cells migrating on lines or unpatterned substrates (Figure 6G). Additionally, staining for focal adhesions revealed that cells on checkerboard patterns have larger focal adhesions than cells on continuous lines (Supplemental Figure S6). While focal adhesions diminished in the region between the leading edge and the nucleus on continuous lines, they remained more prominent on the checkerboard pattern. Taken together, these observations support the hypothesis that cross-talk between newly formed and preexisting focal adhesions limits the increase of traction forces in migrating cells, and that this cross-talk is inhibited in stationary cells by the decreased assembly of new focal adhesions.

DISCUSSION

Using micropatterned polyacrylamide substrates to control cell migration and measure mechanical output simultaneously, we found that stationary cells generated two times stronger traction stress than migrating cells. Similarly, traction stress increased when cells stopped migrating temporarily at the end of a linear track. In addition, the magnitude of traction stress showed an inverse relationship with migration speed on a scatterplot analysis. Control experiments using cells spread within islands of shape and size similar to those of migrating cells excluded different shape or size as the cause for different traction stresses. Together, these observations support the proposal that migration state serves as a regulatory parameter for the output of traction forces.

The inverse relationship between traction stress and migration speed may seem counterintuitive if one considers traction forces solely as a means for driving cell migration. However, traction forces, as well as the associated nascent focal adhesions and filopodia (Wong *et al.*, 2014), have now been implicated as an important means for sensing both mechanical properties of the environment, such as stiffness (Wong *et al.*, 2014), and a cell's own physical state, such as shape and size (Rape *et al.*, 2011b), which may in turn regulate important functions such as differentiation (Engler *et al.*, 2006). Our results further suggest that migration speed serves as an active regulator, rather than a passive outcome, of traction forces, to provide negative feedback to the probing process. Given that migration speed exhibits a biphasic dependence on adhesion strength (DiMilla *et al.*, 1991, 1993; Palecek *et al.*, 1997; Gupton and Waterman-Storer, 2006), cells spread on micropattern islands may be in a state similar to that of cells immobilized on highly adhesive surfaces.

Our results further suggest that the dependence of traction stress on migration state may be related to focal adhesion dynamics. In migrating cells, focal adhesions formed continuously at the leading edge and then moved toward the cell's interior before turning over. This dynamic process is suppressed in stationary cells. An additional clue came from the location of peak traction forces, which were positioned at the very edges of stationary cells but remained at a distance behind the leading edges of migrating cells

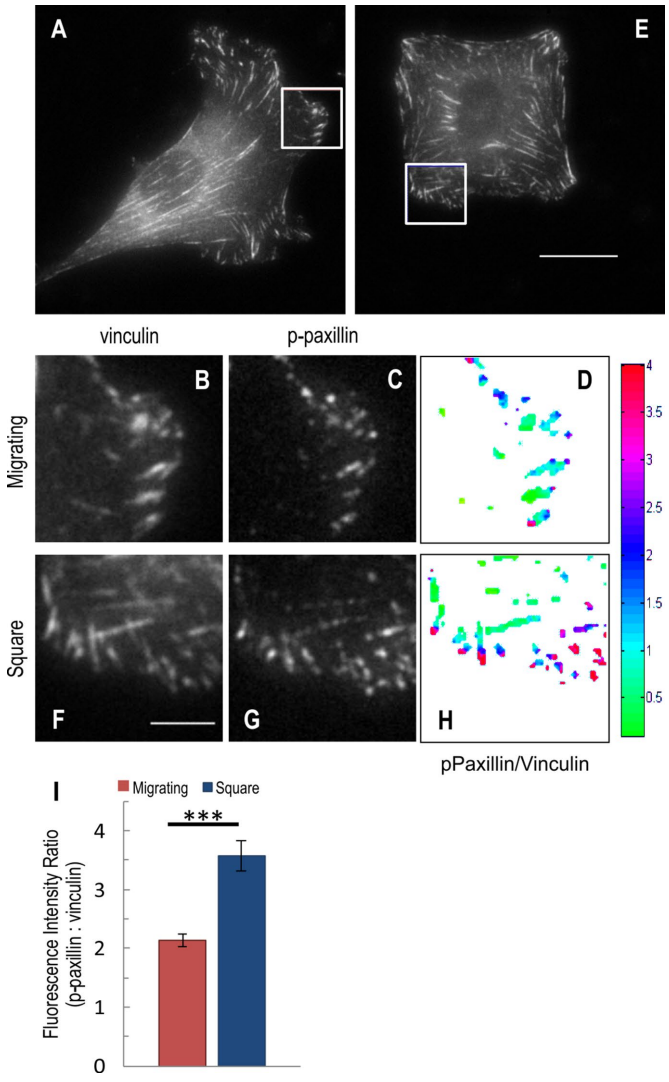

FIGURE 5: Paxillin phosphorylation is sensitive to cell migration state. Vinculin staining showing focal adhesions in migrating (A) and stationary (E) cells serves as the reference for normalization. Scale bar, 20 μm. Boxed regions of interest in migrating (A) and stationary cells (E) are enlarged to show the distribution of vinculin (B, F), and paxillin phosphorylated at Tyr-118 (C, G). Normalized distribution of paxillin phosphorylation is shown as color heat maps of the ratio of intensities between phosphorylated paxillin and vinculin (D, H). A strong presence of phosphor-paxillin is localized along the edge and near the corners of stationary square cells (H, red dots). Scale bar, 5 μm. The average ratio of the intensities of phosphorylated paxillin to those of vinculin is higher for focal adhesions at the corners of stationary cells than for focal adhesions at the leading edges of migrating cells (I); $N = 230$, 300 focal adhesions in migrating and stationary cells respectively. Error bars represent SEM, and *** indicates $p < 0.001$.

in a dynamic manner, supporting the idea that the generation of traction forces was passed continuously to newly formed focal adhesions as a cell moved forward. As a closely related phenomenon, traction force peaked at a distance from the leading edge in rapidly protruding regions but localized close to nonprotruding edges (Stricker *et al.*, 2011).

To explain the strong traction stress underneath nascent rather than mature focal adhesions (Beningo *et al.*, 2001; Stricker *et al.*, 2011), previous studies have proposed an age-based mechanism where focal adhesions lose their mechanical activity as they mature over time (Zaidel-Bar *et al.*, 2004). Our results suggest that this maturation process may involve mechanical interactions between nascent and preexisting focal adhesions located immediately behind. Rearward traction forces exerted on the substrate at the very front would generate forward-pointing counterforces to pull the rest of the cell forward. These forward-pointing forces may counter rear-pointing contractile forces on more interior focal adhesions and trigger their disassembly, given the sensitivity of focal adhesions to mechanical forces (Galbraith *et al.*, 2002). This explanation is supported by the pattern of substrate displacement as cells migrate along checkerboard strips, where inhibition of focal adhesion formation on nonadhesive areas caused traction forces located directly behind to persist (Figure 6, B and C).

A related possibility is that the regulation of focal adhesions is based on both their age and their position and that the mechanochemical environment in the lamellipodia and/or lamellae defines an active zone that facilitates the buildup of traction forces. Cell migration causes focal adhesions to traverse through the active zone, allowing only a finite period of time for traction forces to build up. The faster a cell migrates, the shorter the stay within the active zone and the weaker the traction forces. This sequence of events stops in stationary cells, where traction forces are allowed to build up to a high level as focal adhesions stay within a stationary active zone.

Paxillin phosphorylation is known to increase with increases in contractility (Pasapera *et al.*, 2010), consistent with our observations of concomitant increases of traction stress and phosphorylated paxillin in stationary cells. In addition, paxillin phosphorylation is associated with focal adhesion dynamics (Laukaitis *et al.*, 2001; Zaidel-Bar *et al.*, 2007); thus impaired turnover of focal adhesions in stationary cells may explain the elevated level of paxillin phosphorylation. Focal adhesion kinase (FAK), which plays an important role in rigidity sensing and mechanotransduction (Wang *et al.*, 2001; Tomakidi *et al.*, 2014), is known to interact preferentially with phosphorylated paxillin (Zaidel-Bar *et al.*, 2007), thereby affecting downstream signaling pathways in a migration-dependent manner.

In summary, we suggest a mechanism by which migration state may modulate traction force output, which may in turn affect the ability of cells to organize the extracellular matrix. In addition, different counterforces from the substrate may serve as mechanical signals to regulate intracellular chemical activity. As cell size and shape have been shown to play a pivotal role in regulating both traction forces and stem cell differentiation (McBeath *et al.*, 2004; Kilian *et al.*, 2010), we suspect that the state of migration may play a similar role. For example, differentiation may be suppressed while a cell is migrating during development, to be activated only when the cell has arrived at the destination. Likewise, defects in the response to migration state may cause cancer cells to lose control over their own growth and differentiation.

MATERIALS AND METHODS

Substrate preparation

Micropatterned polyacrylamide hydrogels were prepared as described previously (Rape *et al.*, 2011b). Briefly, a polydimethylsiloxane stamp was incubated for 45 min with a 0.1% (wt/vol) gelatin solution that had been activated with 3.5 mg/ml sodium periodate (Sigma, St. Louis, MO). The stamp was dried using N_2 gas and then lightly pressed onto a small glass coverslip. A freshly prepared solution of 5% acrylamide and 0.1% bis-acrylamide (Bio-Rad, Hercules, CA) was degassed and mixed with 0.2-μm fluorescent beads (Molecular Probes, Carlsbad, CA) at a 2000:1 ratio for traction force

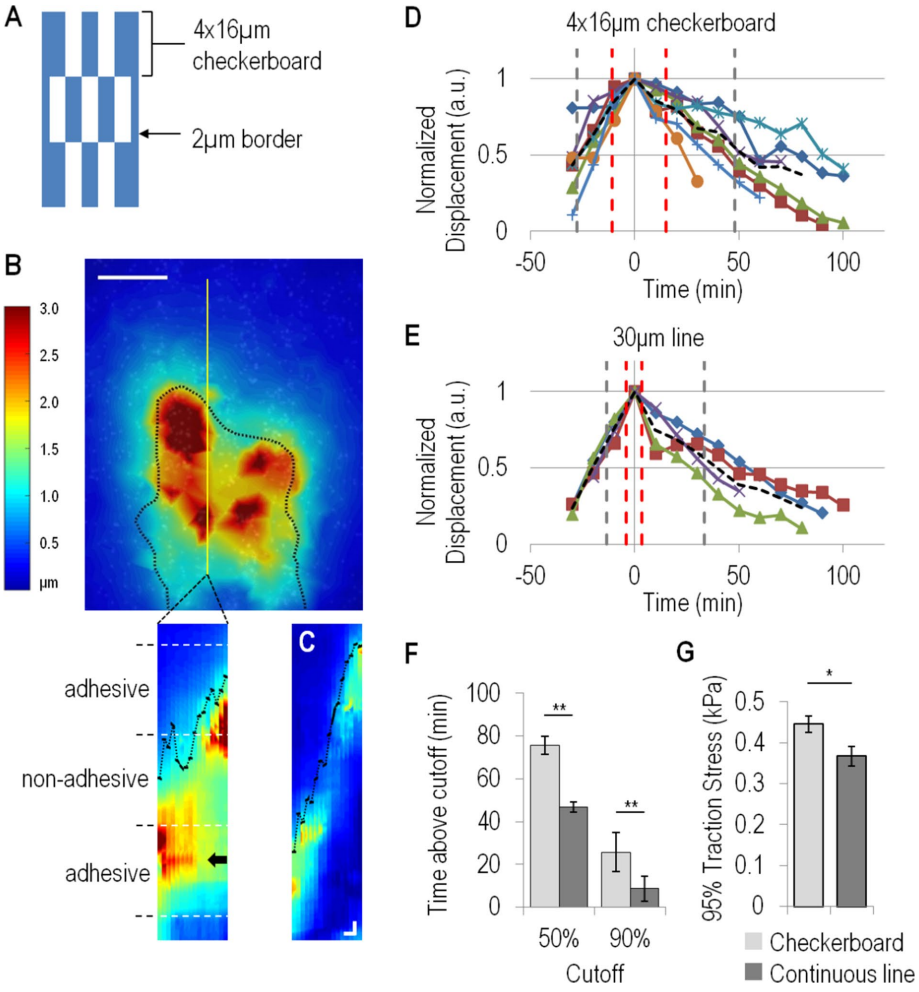

FIGURE 6: Adhesions at the front are associated with the decrease of traction forces behind. NIH 3T3 cells are allowed to migrate along strips with a checkerboard pattern consisting of 4 × 16–μm rectangular adhesive areas (A, adhesive areas in blue). Heat maps depict substrate displacement caused by cells migrating along the pattern (B). Scale bar, 10 μm. Dotted black line represents cell outline. Yellow solid line indicates the region of interest for generating kymographs as the cell migrates across alternating adhesive and nonadhesive regions (bottom left panel). Black arrow indicates where substrate displacement persists while the leading edge migrates across a nonadhesive region (B, bottom panel). For cells migrating along continuous adhesive strips 30 μm in width, substrate displacement is more transient, as indicated by the short length of displacement peaks along the time axis (C, plotted using the same color scale as B). Duration of kymograph, 1 h. Displacements at fixed sites are plotted as a function of time for cells migrating along checkerboards (D; $N = 7$) and continuous lines (E; $N = 4$), respectively. Red dotted lines denote the time when the average displacement rises or falls to 90% of the maximum, and gray dotted lines denote the time when the average displacement (D, E, black dotted line) rises or falls to 50% of the maximum displacement. Cells migrating along checkerboard-patterned strips (D, F) show slower decay kinetics than cells migrating along continuous strips (E, F). Cells also exert higher 95% traction stress on checkerboard patterns (G, $N = 28, 20$; data for the continuous line taken from Figure 1). Error bars represent SEM. ** indicates $p < 0.01$. * indicates $p < 0.05$.

microscopy. After addition of the initiators ammonium persulfate (Sigma) and *N,N,N′,N′*-tetramethylethane-1,2-diamine (EMD Millipore, Billerica, MA), a 30-μl drop was pipetted onto a large coverslip pretreated with Bind-Silane (GE Healthcare, Little Chalfont, United Kingdom). The small coverslip with stamped pattern was immediately placed pattern side down on the acrylamide drop. After complete acrylamide polymerization over 20–40 min, the top coverslip was carefully removed with a pair of fine forceps. Micropatterned polyacrylamide hydrogel substrates were mounted into chamber dishes, sterilized under ultraviolet light for 30 min, and incubated in cell culture media at 37°C for 1 h before use. The final gel had an estimated Young's modulus of 3.5 kPa (Tse and Engler, 2010). Checkerboard patterns were designed as shown in Figure 6 with alternating 4 × 16–μm adhesive and nonadhesive areas flanked by a 2-μm-wide adhesive border. In addition, a teardrop pattern was designed to generate an area and shape similar to those of cells on unpatterned surfaces.

Glass substrates micropatterned with linear polyacrylamide to generate nonadhesive areas were prepared as described previously (Guo and Wang, 2011). Briefly, a coverslip was treated with Bind-Silane. Standard photolithography techniques were used to cover/protect areas designated for cell adhesion with SPR 220.3 positive photoresist (Microchem, Newton, MA). The remaining glass surface was rendered nonadhesive by grafting linear polyacrylamide onto it. The photoresist was then stripped away using Remover 1165 (Microchem), and the exposed glass surface was incubated with 10 μg/ml fibronectin (Sigma) for 1 h before cell inoculation.

Cell culture

NIH 3T3 cells (American Type Culture Collection, Manassas, VA) were cultured in DMEM (Life Technologies, Carlsbad, CA) supplemented with 10% donor adult bovine serum (Thermo Scientific, Waltham, MA), 2 mM L-glutamine, 50 μg/ml streptomycin, and 50 U/ml penicillin (Life Technologies) and were maintained under 5% CO_2 at 37°C. The mCherry–paxillin construct was kindly provided by Michael Davidson (Florida State University). Cells were transfected using the Amaxa Nucleofector (Lonza, Walkersville, MD) following the manufacturer's instructions.

Traction force microscopy

Phase contrast images of single cells spread on a uniformly coated polyacrylamide gel or across a micropatterned island were collected with a Nikon Eclipse Ti microscope and a 40× N.A. 0.75 Plan-Fluor dry objective (Nikon, Melville, NY), using an Andor iXon EMCCD camera (Northern Ireland, UK) and custom software. Fluorescent images of the embedded beads near the surface of the hydrogel were taken before and after cells were removed with 0.05% Trypsin-EDTA (Life Technologies). For time-lapse recordings, paired phase-contrast images of the cell and fluorescence images of the underlying beads were collected every 10 min for 4 h. For high-resolution tracking of substrate strain, phase contrast and corresponding fluorescence images were collected using a 100× N.A. 1.3 Plan Fluor oil immersion objective (Nikon) every 4 min for up

to 2 h. Cell outlines were drawn manually, and bead displacement fields were computed using custom software. Color heat maps of traction force-induced strains were generated using MATLAB. Plots of substrate displacement were generated in regions showing strong substrate displacement. The displacements were normalized to a range of 0–1 and averaged within local regions to generate the plots shown in Figure 6, D and E. Traction stress and strain energy were computed using the LIBTRC software package (Micah Dembo, Boston University).

Total internal reflection fluorescence microscopy and analysis of focal adhesion dynamics

Cells expressing mCherry–paxillin were plated on glass substrates incubated with fibronectin. TIRF images of focal adhesions in cells spread on either a 50 × 50–μm square micropattern or an unpatterned coverslip were collected with a Nikon Eclipse Ti microscope using a 100× N.A. 1.49 Apo TIRF oil immersion objective (Nikon) and an Andor iXon EMCCD camera. mCherry was excited using a 561-nm laser (Coherent, Santa Clara, CA) and images were collected every 4 min for 2 h. Focal adhesion area was quantified using the Focal Adhesion Analysis Server (FAAS; Berginski and Gomez, 2013). Settings used for the FAAS were as follows: detection threshold = 1, minimum adhesion size = 2 pixels (~0.05 μm^2), maximum adhesion size = none, frame cutoff number = 1, minimum aspect ratio = 1. Corners of square cells were defined as a 15 × 15–μm region of interest at each of the four corners. Lifetime of focal adhesions that formed at the leading edge of migrating cells and at the corners of stationary cells was manually measured using time-lapse images and include adhesions detected by the FAAS software that persisted for at least two consecutive frames. Unless otherwise indicated, statistical analysis was performed using a *t* test with the Bonferroni correction for multiple comparisons.

Immunostaining

Cells seeded on micropatterned polyacrylamide substrates were fixed in 4% formaldehyde (Thermo Scientific) and stained with mouse monoclonal antibodies against vinculin (Santa Cruz Biotechnology sc-73614, Dallas, TX) and rabbit polyclonal antibodies against Tyr-118 phosphorylated paxillin (Cell Signaling Technology #2541, Danvers, MA). Ser-19–phosphorylated myosin II regulatory light chain was stained with a mouse monoclonal antibody (Cell Signaling Technology #3675) at a dilution of 1:200.

Fluorescent images were collected using a 40× N.A. 0.75 PlanFluor objective lens for phosphorylated myosin regulatory light chain, or a 100× N.A. 1.3 PlanFluor oil immersion objective lens otherwise. Average background intensity was subtracted from each image using custom software. Fluorescence intensity of phosphorylated paxillin was divided by that of vinculin at 10 focal adhesions near the leading edge of each cell showing the strongest phosphorylated paxillin fluorescence signals. Focal adhesions were segmented to create a mask in ImageJ. The masks were used in creating color heat maps of the ratio of phosphorylated paxillin to vinculin fluorescence using MATLAB.

ACKNOWLEDGMENTS

We thank Micah Dembo at Boston University for providing the LIBTRC software package for computing traction stress and Michael Davidson at Florida State University for providing the mCherry–paxillin constructs. This work was funded by Grants GM32476 and GM118998 from the National Institutes of Health to Y.L.W.

REFERENCES

Baker BM, Chen CS (2012). Deconstructing the third dimension: how 3D culture microenvironments alter cellular cues. J Cell Sci 125, 3015–3024.

Beningo KA, Dembo M, Kaverina I, Small JV, Wang YL (2001). Nascent focal adhesions are responsible for the generation of strong propulsive forces in migrating fibroblasts. J Cell Biol 153, 881–888.

Berginski ME, Gomez SM (2013). The Focal Adhesion Analysis Server: a Web tool for analyzing focal adhesion dynamics. F1000Research 2, 68.

Chang SS, Guo WH, Kim Y, Wang YL (2013). Guidance of cell migration by substrate dimension. Biophys J 104, 313–321.

Choi CK, Zareno J, Digman MA, Gratton E, Horwitz AR (2011). Cross-correlated fluctuation analysis reveals phosphorylation-regulated paxillin–FAK complexes in nascent adhesions. Biophys J 100, 583–592.

Dembo M, Wang YL (1999). Stresses at the cell-to-substrate interface during locomotion of fibroblasts. Biophys J 76, 2307–2316.

DiMilla PA, Barbee K, Lauffenburger DA (1991). Mathematical model for the effects of adhesion and mechanics on cell migration speed. Biophys J 60, 15–37.

DiMilla PA, Stone JA, Quinn JA, Albelda SM, Lauffenburger DA (1993). Maximal migration of human smooth muscle cells on fibronectin and type-IV collagen ocurs an intermediate attachment strenght. J Cell Biol 122, 729–737.

Discher DE, Janmey P, Wang YL (2005). Tissue cells feel and respond to the stiffness of their substrate. Science 310, 1139–1143.

Engler AJ, Sen S, Sweeney HJ, Discher DE (2006). Matrix elasticity directs stem cell lineage specification. Cell 126, 677–689.

Galbraith CG, Yamada KM, Sheetz MP (2002). The relationship between force and focal complex development. J Cell Biol 159, 695–705.

Geiger B, Spatz JP, Bershadsky AD (2009). Environmental sensing through focal adhesions. Nat Rev Mol Cell Biol 10, 21–33.

Guo W, Wang YL (2011). Micropatterning cell–substrate adhesions using linear polyacrylamide as the blocking agent. Cold Spring Harb Protoc, doi:10.1101/pdb.prot5582.

Gupton SL, Waterman-Storer CM (2006). Spatiotemporal feedback between actomyosin and focal-adhesion systems optimizes rapid cell migration. Cell 125, 1361–1374.

Kilian K, Bugarija B, Lahn BT, Mrksich M (2010). Geometric cues for directing the differentiation of mesenchymal stem cells. Proc Natl Acad Sci USA 107, 4872–4877.

Kraning-Rush CM, Califano JP, Reinhart-King CA (2012). Cellular traction stresses increase with increasing metastatic potential. PLoS One 7, e32572.

Laukaitis CM, Webb DJ, Donais K, Horwitz AF (2001). Differential dynamics of α5 integrin, paxillin, and α-actinin during formation and disassembly of adhesions in migrating cells. J Cell Biol 153, 1427–1440.

Lo CM, Wang H, Dembo M, Wang YL (2000). Cell movement is guided by the rigidity of the substrate. Biophys J 79, 144–152.

McBeath R, Pirone DM, Nelson CM, Bhadriraju K, Chen CS (2004). Cell shape, cytoskeletal tension, and RhoA regulate stem cell lineage commitment. Dev Cell 6, 483–495.

Morin TR, Ghassem-Zadeh SA, Lee J (2014). Traction force microscopy in rapidly moving cells reveals separate roles for ROCK and MLCK in the mechanics of retraction. Exp Cell Res 326, 280–294.

Munevar S, Wang YL, Dembo M (2001). Traction force microscopy of migrating normal and H-ras transformed 3T3 fibroblasts. Biophys J 80, 1744–1757.

Oakes PW, Banerjee S, Marchetti MC, Gardel ML (2014). Geometry regulates traction stresses in adherent cells. Biophys J 107, 825–833.

Palecek SP, Loftus JC, Ginsberg MH, Lauffenburger DA, Horwitz AF (1997). Integrin–ligand binding properties govern cell migration speed through cell–substratum adhesiveness. Nature 385, 537–340.

Parker KK, Brock AL, Brangwynne C, Mannix RJ, Wang N, Ostuni E, Geisse NA, Adams JC, Whitesides GM, Ingber DE (2002). Directional control of lamellipodia extension by constraining cell shape and orienting cell tractional forces. FASEB J 16, 1195–1204.

Pasapera AM, Schneider IC, Rericha E, Schlaepfer DD, Waterman CM (2010). Myosin II activity regulates vinculin recruitment to focal adhesions through FAK-mediated paxillin phosphorylation. J Cell Biol 188, 877–890.

Prager-Khoutorsky M, Lichtenstein A, Krishnan R, Rajendran K, Mayo A, Kam Z, Geiger B, Bershadsky AD (2011). Fibroblast polarization is a matrix-rigidity-dependent process controlled by focal adhesion mechanosensing. Nat Cell Biol 13, 1457–1465.

Raman PS, Paul CD, Stroka KM, Konstantopoulos K (2013). Probing cell traction forces in confined microenvironments. Lab Chip 13, 4599-4607.
Rape AD, Guo WH, Wang YL (2011a). Responses of cells to adhesion-mediated signals: a universal mechanism. In: Mechanobiology of Cell–Cell and Cell–Matrix Interactions, ed. JA Wagoner and BAC Harley, Boston: Springer US, 1–10.
Rape AD, Guo WH, Wang, YL (2011b). The regulation of traction force in relation to cell shape and focal adhesions. Biomaterials 32, 2043–2051.
Smilenov LB, Mikhailov A, Pelham RJ, Marcantonio EE, Gundersen GG (1999). Focal adhesion motility revealed in stationary fibroblasts. Science 286, 1172–1174.
Stricker J, Aratyn-Schaus Y, Oakes PW, Gardel ML (2011). Spatiotemporal constraints on the force-dependent growth of focal adhesions. Biophys J 100, 2883–2893.
Tomakidi P, Schulz S, Proksch S, Weber W, Steinberg T (2014). Focal adhesion kinase (FAK) perspectives in mechanobiology: implications for cell behaviour. Cell Tissue Res 357, 515–526.
Trichet L, Le Digabel J, Hawkins RJ, Vedula SRK, Gupta M, Ribrault C, Hersen P, Voituriez R, Ladoux B (2012). Evidence of a large-scale mechanosensing mechanism for cellular adaptation to substrate stiffness. Proc Natl Acad Sci USA 109, 6933–6938.
Tse JR, Engler AJ (2010). Preparation of hydrogel substrates with tunable mechanical properties. Curr Protocol Cell Biol 47, 10.16.1–10.16.16.
Vicente-Manzanares M, Choi CK, Horwitz AR (2009). Integrins in cell migration—the actin connection. J Cell Sci 122, 199–206.
Vogel V, Sheetz M (2006). Local force and geometry sensing regulate cell functions. Nat Rev Mol Cell Biol 7, 265–275.
Wang HB, Dembo M, Hanks SK, Wang YL (2001). Focal adhesion kinase is involved in mechanosensing during fibroblast migration. Proc Natl Acad Sci USA 98, 11295–11300.
Wang HB, Dembo M, Wang YL (2000). Substrate flexibility regulates growth and apoptosis of normal but not transformed cells. Am J Physiol Cell Physiol 279, C1345–C1350.
Wang, N, Ostuni E, Whitesides GM, Ingber DE (2002). Micropatterning tractional forces in living cells. Cell Motil Cytoskeleton 52, 97–106.
Wong S, Guo WH, Wang YL (2014). Fibroblasts probe substrate rigidity with filopodia extensions before occupying an area. Proc Natl Acad Sci USA 111, 17176–17181.
Zaidel-Bar R, Cohen M, Addadi L, Geiger B (2004). Hierarchical assembly of cell–matrix adhesion complexes. Biochem Soc Trans 32, 416–420.
Zaidel-Bar R, Milo R, Kam Z, Geiger B (2007). A paxillin tyrosine phosphorylation switch regulates the assembly and form of cell–matrix adhesions. J Cell Sci 120, 137–148.